Strong Extinction of a Laser Beam by a Single Molecule

I. Gerhardt, G. Wrigge, P. Bushev, G. Zumofen, M. Agio, R. Pfab, and V. Sandoghdar*

Laboratory of Physical Chemistry, ETH Zurich, CH-8093 Zurich, Switzerland

(Received 13 April 2006; published 17 January 2007)

We present an experiment where a single molecule strongly affects the amplitude and phase of a laser field emerging from a subwavelength aperture. We achieve a visibility of -6% in direct and $+10\%$ in cross-polarized detection schemes. Our analysis shows that a close to full extinction should be possible using near-field excitation.

DOI: 10.1103/PhysRevLett.98.033601 PACS numbers: 42.50.Gy, 42.50.Nn, 42.62.Fi, 68.37.Uv

The strength of the interaction between radiation and matter is often formulated in terms of a cross section, modeling the object as a disk of a certain area exposed to the radiation. For an ideal oriented quantum mechanical two-level system with a transition wavelength λ, the absorption cross section amounts to $\sigma_{\mathrm{abs}} = 3\lambda^2/2\pi$ [1]. This formulation suggests that a single emitter would fully extinguish the incident light if one could only focus it to an area smaller than σ_{abs}. In fact, it is possible to confine a laser beam to an area of about $(\lambda/2\mathrm{NA})^2$, using immersion optics with a high numerical aperture (NA) or to confine it to a subwavelength area using scanning near-field optical microscopy (SNOM). However, it turns out that it is a nontrivial task to explore these ideas experimentally because systems in the gas phase are not easily compatible with strongly confined laser fields [2]. Moreover, solid-state emitters suffer from broad homogeneous linewidths (γ) at room temperature, reducing σ_{abs} by the factor γ_0/γ where γ_0 is the radiative linewidth [1]. Considering these constraints, we have chosen to use a cryogenic SNOM and have succeeded in detecting single molecules in transmission with a visibility of up to 10%, which we present in this Letter. We also discuss possible applications and impact of our work in the latter part of our presentation.

Optical detection of single solid-state emitters was pioneered by applying a double modulation technique in absorption spectroscopy [3]. In that work molecules doped in an organic crystal were excited via the narrow zero-phonon lines of the $1 \rightarrow 2$ transition [see Fig. 1(b)] at liquid helium temperature, and a laser focus of 3 μm yielded an absorption effect of about 10^{-4}. Soon after that it was shown that the detection signal-to-noise ratio (SNR) would be much more favorable if one performed fluorescence excitation spectroscopy to collect the Stokes shifted emission of the molecule (transition $2 \rightarrow 3$) while blocking the excitation beam with filters [4]. In fact, this mode of spectroscopy was also performed using a near-field tip [5]. Unfortunately, however, this method sacrifices the information about coherent processes at the frequency ν_{21}. A few recent works have used the interference between the coherent radiation of a single emitter and a part of the excitation beam in reflection to get around this issue [6,7]. Here we extend the latter idea to direct transmission measurements.

Figure 1(a) shows the schematics of the experimental arrangement based on a combined cryogenic confocal/near-field microscope operating at $T = 1.4$ K [8]. Light from a tunable dye laser ($\lambda \sim 615$ nm, linewidth $\sim$ 1 MHz) was coupled into a single mode fiber leading to the SNOM tip in the cryostat. The SNOM probes were fabricated by evaporating aluminum onto heat-pulled fiber tips and subsequent focused ion beam milling of their ends to produce apertures of about 100 nm [see Fig. 1(c)]. The tip could be positioned in front of the sample using home-built piezo-electric sliders. The shear force signal using a quartz tuning fork was used to determine the point of contact between the tip and the sample to within 10 nm. The sample could be scanned in 3 dimensions using a commercial piezo-electric stage. The light transmitted through the tip or emitted by the molecules was collected by a microscope objective (NA = 0.8) which could also be

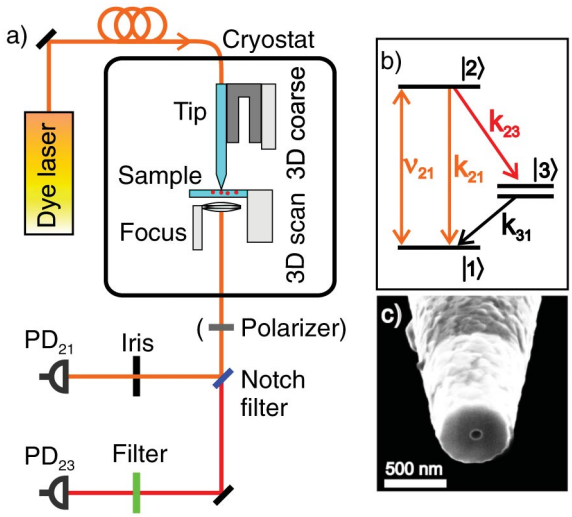

FIG. 1 (color). (a) Schematics of the experimental setup. The polarizer was inserted for the data in Fig. 3; for details see text. (b) The molecular energy level scheme. ν_{12} denotes the zero-phonon line frequency of the 0-0 vibrational transition. k_{21} describes the decay rate of $|2\rangle$ to $|1\rangle$, which includes both the zero-phonon and the phonon-wing transitions. Manifold $|3\rangle$ signifies the Stokes shifted vibrational levels of the electronic ground state. (c) An electron microscope image of a typical SNOM probe.

translated by a slider. Filters and beam splitters were used to direct the radiation of the $2 \rightarrow 1$ transition (of the order of 40% of the total emission) to the avalanche photodiode PD_{21} and the Stokes shifted fluorescence to PD_{23}. In the experiments discussed in this work, an iris with an opening of about 1 mm selected the central 10% of the forward emission in the PD_{21} path.

Crystalline films of *p*-terphenyl doped with dibenzanthanthrene (DBATT) molecules [9] were fabricated on a glass coverslip by spin coating [10]. After an annealing step, the resulting sample contained large regions of *p*-terphenyl with typical heights of 50–100 nm, thin enough to allow near-field studies. By performing room temperature experiments, we determined the transition dipole moments of the DBATT molecules to lie at an angle of about $25 \pm 5°$ with respect to the tip axis and measured the fluorescence lifetime of level $|2\rangle$ to be 20 ± 3 ns, corresponding to a full width at half-maximum linewidth of $\gamma_0 = 8 \pm 1$ MHz.

In a given experimental run, we first used fluorescence excitation spectroscopy to identify the zero-phonon transition frequencies of the molecules located under the tip aperture. Next we adjusted the tip-sample separation to about 60 nm and optimized the fluorescence signal I_{23} from the molecule by laterally positioning the sample in the x and y directions. Figure 2(a) shows a near-field fluorescence excitation spectrum measured on PD_{23}. Figure 2(b) displays the signal on PD_{21} recorded simultaneously with the first spectrum, revealing an impressive drop of 6% in the incident beam power due to the presence of a single molecule. The SNR of 20 was obtained with an integration time per pixel of 10 ms and averaging of 20 scans. The laser intensity in the tip was stabilized to 0.3% by monitoring a slight light leakage around a fiber bend in the cryostat.

The transmission spectrum recorded on PD_{21} suggests that, as expected intuitively and formulated in recent literature [11], the incident light is "absorbed" by the molecule on resonance. However, scattering theory [1,12] tells us that the signal I_d on the detector PD_{21} is due to the interference of the electric fields of the excitation light E_e and the radiation emitted by the molecule E_m. Using the operator notation common in quantum optics [1], we can write

$$I_d = \langle \hat{\mathbf{E}}_e^- \cdot \hat{\mathbf{E}}_e^+ \rangle + \langle \hat{\mathbf{E}}_m^- \cdot \hat{\mathbf{E}}_m^+ \rangle + 2\,\mathrm{Re}\{\langle \hat{\mathbf{E}}_e^- \cdot \hat{\mathbf{E}}_m^+ \rangle\}. \quad (1)$$

The first term represents the intensity I_e of the excitation light on the detector. The part of the electric field E_m on PD_{21} is composed of two contributions, $E_m = E_{21}^c + E_{21}^{ic}$. The first component represents the coherent elastic (Rayleigh) scattering process of a well-defined phase with respect to the incident laser beam. The second term takes into account an incoherent part which is produced by the inelastic interactions between the excitation light and the upper state of the molecule [1] as well as the emission in the phonon wing of the $2 \rightarrow 1$ transition due to its phonon coupling with the matrix [13]. Thus the second component of Eq. (1) represents the molecular emission intensity $I_{21}^c + I_{21}^{ic}$. The last term of Eq. (1) is responsible for the interference between the excitation field and the coherent part of the molecular emission E_{21}^c and is often called the "extinction" term [12]. It follows that if E_m is much weaker than E_e, the extinction term dominates the direct molecular emission intensity.

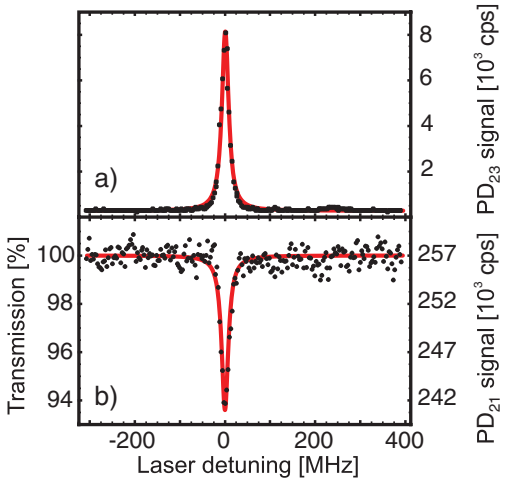

FIG. 2 (color). Symbols show simultaneously recorded near-field fluorescence excitation (a) and transmission (b) spectra. The solid red curves display fits. In the legend of the right vertical axis, cps stands for counts per second.

We now develop a quantitative description of the transmission signal on PD_{21}, keeping in mind the vectorial nature and polarization properties of the light fields. The excitation electric field along the unit vector $\mathbf{u}_d$ at position $\mathbf{r}$ of the detector can be written as

$$\langle \hat{\mathbf{E}}_e^+(\mathbf{r}) \rangle = [\langle \hat{\mathbf{E}}_e^+(\mathbf{r}_m) \rangle \cdot \mathbf{u}_m] g \mathbf{u}_d. \quad (2)$$

Here $\mathbf{r}_m$ is the position of the molecule, and $\mathbf{u}_m$ is a unit vector along its transition dipole moment. We have introduced $g = |g| e^{i\phi_g}$ as a complex modal factor that accounts for the amplitude, phase, and polarization of the tip emission through the detection path, starting from the projection of $\mathbf{E}_e$ on $\mathbf{u}_m$ and ending at $\mathbf{u}_d$. The electric field of the coherently scattered light is given by [1]

$$\langle \hat{\mathbf{E}}_{21}^{c+}(\mathbf{r}) \rangle = (\sqrt{\alpha} d_{21}) \rho_{21} f \mathbf{u}_d. \quad (3)$$

The quantity $d_{21} = \langle 2|\hat{D}|1\rangle$ is the matrix element of the dipole operator. In a solid-state system, the intensity of the zero-phonon line is typically reduced by the Debye-Waller factor α due to emission into the phonon wing [13]. The dipole moment corresponding to the zero-phonon transition, therefore, is given by $\sqrt{\alpha} d_{21}$. Our preliminary measurements for DBATT in *p*-terphenyl thin films let us estimate $\alpha = 0.25 \pm 0.05$. Furthermore, adapting the standard textbook treatment of resonance fluorescence to a three level system, we find for the steady-state density matrix element ρ_{21},

$$\rho_{21} = \frac{\Omega(-\Delta + i\gamma/2)}{2} \mathcal{L}(\nu) \quad (4)$$

with

$$\mathcal{L}(\nu) = \frac{1}{\Delta^2 + \gamma^2/4 + \Omega^2(\gamma/2\gamma_0)K} \simeq \frac{1}{\Delta^2 + \gamma^2/4} \quad (5)$$

where $\Delta = \nu - \nu_{21}$ is the detuning between the laser frequency ν and the zero-phonon frequency ν_{21}. The quantity $\Omega = (\sqrt{\alpha}d_{21})[\langle \hat{\mathbf{E}}_e^+(\mathbf{r}_m)\rangle \cdot \mathbf{u}_m]/h$ stands for the Rabi frequency. We have verified that all our measurements are in the regime well below saturation so that $\Omega \ll \gamma$. The parameter $K = 1 + k_{23}/2k_{31}$ accounts for the competition of various decay rates k_{21}, k_{23}, and k_{31} [see Fig. 1(b)]. In our case $k_{31} \gg k_{23}$ so that $K \simeq 1$. These considerations result in the last form of the expression in Eq. (5). Finally, in Eq. (3) we have introduced $f = |f|e^{i\phi_f}$ similar to g, as a complex modal factor that determines the angular dependence, the phase, and polarization of the molecular field at the detector, taking into account the effect of the substrate interfaces and of the tip. However, contrary to g, we have included some dimensional parameters in f to simplify the presentation of our formulae.

After some simple algebra [14], one can show that

$$I_d = I_e\left[1 + \alpha d_{21}^4 \frac{\gamma}{4\gamma_0}\left|\frac{f}{g}\right|^2 \mathcal{L}(\nu) - \alpha d_{21}^2 \left|\frac{f}{g}\right| \mathcal{L}(\nu)\left(\Delta\cos\psi + \frac{\gamma}{2}\sin\psi\right)\right] \quad (6)$$

for the forward direction. The phase angle $\psi = \phi_f - \phi_g$ denotes the accumulated phase difference between the radiation of the molecule and of the SNOM tip on the detector after propagation through the whole optical system. By determining I_e from the off-resonant part of the spectra and γ from the simultaneously recorded $I_{23}(\nu)$, we have fitted our frequency scans using Eq. (6), whereby we have used ψ and the multiplicative factor $d_{21}^2|f/g|$ as free parameters. An example is shown by the red solid curve in Fig. 2(b) where we obtained $\psi = \pi/2$. It is also possible to vary ψ to obtain dispersive shapes or even peaks. One way of achieving this is to scan the tip in the x, y, and z directions. Our results on such studies and on the influence of the tip on I_d will be published separately [15]. In what follows, we show how the observed signal could be changed by selecting different polarizations in the detection path. Furthermore, we define the visibility $V(\nu) = (I_d - I_e)/I_e$ of the detected signal and will discuss how the change in the ratio $|f/g|$ of the modal factors influences the observed visibility.

Figure 3 shows the polarization dependence of the SNOM emission and the Stokes shifted fluorescence on the two detectors when a linear polarizer was placed after the cryostat [see Fig. 1(a)]. We find that the main polarization axes of E_e and E_{23} are offset by about 20°. The weak polarization extinction ratio (2:1) of I_{23} stems mostly from the component of the molecular dipole along the optical axis which gives rise to radially polarized fields at the outer part of the detected beam [16]. Furthermore, the dielectric mirrors in the detection path [not shown in Fig. 1(a)] introduce a non-negligible degree of ellipticity to the polarization. Note that since the polarization properties of the fields E_{23} and E_{21}^c of the molecule are both determined by the orientation of its dipole moment, the dashed lines in Fig. 3 also provide information on the polarization of E_{21}^c.

In Fig. 4(a) we present $V(\nu)$ recorded on PD_{21} for a series of polarizer angles θ whereby $\theta = 0$ marks the highest I_e. Here we have adapted the integration times for each θ to keep roughly the same SNR. As θ changes, the spectrum evolves from an absorptive to a dispersive shape, revealing a variation in $\psi = \phi_f - \phi_g$. The data points in Fig. 4(b) display an example for $\theta = 75°$. The rotation of the polarizer results in the projection of E_e and E_{21}^c onto different detection polarizations $\mathbf{u}_d$, which in turn implies variations of g and f. In particular, ψ is changed if the fields possess some ellipticity. Indeed, by extracting the degree of ellipticity from the polarization data in Fig. 3, we have been able to fit the recorded spectra in Fig. 4(a) simultaneously for all θ using Eq. (6).

As displayed in Fig. 4(c), a remarkable situation results for the cross-polarized detection ($\theta = 90°$) where the visibility reaches +10% on resonance, yielding $\psi \simeq 3\pi/2$. This surplus of light on resonance is a clear signature of interference and redistribution of light. In fact, we have verified that the sum of the spectra recorded at θ and $\theta + \pi/2$ remains constant and absorptive for all θ. The fact that V is larger here than in Fig. 2(b) although I_d is diminished to 1/20 of its original value, can be readily explained by Eq. (6) where reducing g causes an increase in V. It is furthermore interesting to note that if g approaches zero, the second term in Eq. (6) dominates, giving access to the direct emission on the $2 \rightarrow 1$ transition. The physical origin and the optimization of I_d and V, therefore, depend on the ratio $|f/g|$.

We now discuss various aspects of our results and their prospects for future studies. Based on the data in Fig. 2(b), a contrast of 1% on an incident power of $I_e = 250 \times 10^3$ counts per second (cps), is easily measurable, corresponding to a very low coherent emission of $I_{21}^c = 25$ cps. Thus, our experimental approach makes it possible to detect weakly fluorescing emitters. Moreover, since the extinc-

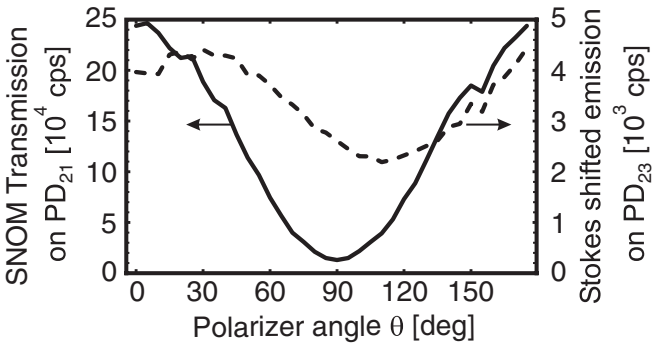

FIG. 3. Tip emission and Stokes shifted molecular fluorescence for different orientations of polarizer in the detection.

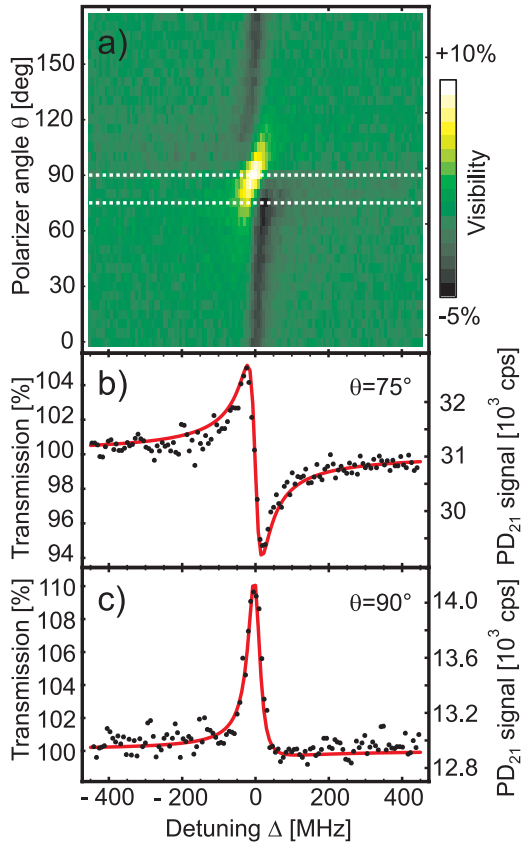

FIG. 4 (color). (a) Frequency spectra recorded on PD_{21} for 30 polarizer angles spanning 180°. The visibility is color coded. (b), (c) Cross sections from (a) for $\theta = 75°$ and $\theta = 90°$ with fit functions according to Eq. (6).

tion term in Eq. (6) is proportional to α/γ on resonance, $\gamma_0 = 8 \pm 1$ MHz, and $\gamma = 35$ MHz (see Fig. 2), we conclude that V could have been $\gamma/(\alpha\gamma_0) \simeq 16$ times larger, approaching 100%.

We emphasize that the visibility V defined above is not a direct measure of the absorption cross section that is conventionally defined for a plane wave excitation. A rigorous treatment of the absorption cross section for near-field excitation should take into account the inhomogeneous distribution of the vectorial excitation and molecular fields, as well as the tip and sample geometries [17], and it remains a topic of future study. Here it suffices to point out that the key advantage in near-field coupling is that the field lines of the SNOM tip or a nanoscopic antenna [18] are well matched to those of a dipolar emitter, resulting in a better mode overlap than that achievable in far-field optics [19]. In this work, we have considered the forward propagation through an iris [see Fig. 1(a)]. However, by replacing the avalanche photodiode with a sensitive camera, it is possible to map the complex mode overlap between E_m and E_e. We are currently pursuing such measurements.

The experiments presented here were performed on many samples, molecules, and tips, and visibilities above 2% were consistently obtained. To the best of our knowledge, an extinction of 6% and a surplus signal of 10% are the largest effects yet reported for a single emitter acting directly on a light beam. The interferometric nature of our detection scheme provides access to the coherent optical phenomena in a single solid-state emitter. Furthermore, the efficient near-field absorption spectroscopy technique presented here can be used to study weakly fluorescing nanoobjects or single emitters that do not have large Stokes shifts. Moreover, our work might find applications in single atom detection on atom chips [20]. Finally, a direct and strong coupling of light to a single emitter allows an efficient manipulation of its phase and amplitude, which are considered to be key elements for the execution of various quantum optical tasks [21].

We thank A. Renn, C. Hettich, and S. Kühn for experimental support. This work was financed by the Schweizerische Nationalfond and the ETH Zurich initiative for Quantum Systems for Information Technology (QSIT).

*Electronic address: vahid.sandoghdar@ethz.ch

[1] R. Loudon, *Quantum Theory of Light* (Oxford University Press, New York, 2000).
[2] D. J. Wineland, W. M. Itano, and J. C. Bergquist, Opt. Lett. **12**, 389 (1987).
[3] W. E. Moerner and L. Kador, Phys. Rev. Lett. **62**, 2535 (1989).
[4] M. Orrit and J. Bernard, Phys. Rev. Lett. **65**, 2716 (1990).
[5] W. E. Moerner *et al.*, Phys. Rev. Lett. **73**, 2764 (1994).
[6] T. Plakhotnik and V. Palm, Phys. Rev. Lett. **87**, 183602 (2001).
[7] B. Alen *et al.*, cond-mat/0509114v1.
[8] J. Michaelis, C. Hettich, J. Mlynek, and V. Sandoghdar, Nature (London) **405**, 325 (2000).
[9] A.-M. Boiron, B. Lounis, and M. Orrit, J. Chem. Phys. **105**, 3969 (1996).
[10] R. J. Pfab *et al.*, Chem. Phys. Lett. **387**, 490 (2004).
[11] J. R. Guest *et al.*, Phys. Rev. B **65**, 241310(R) (2002).
[12] D. Jackson, *Classical Electrodynamics* (Wiley and Sons, New York, 1999).
[13] M. Orrit, J. Bernard, and R. I. Personov, J. Phys. Chem. **97**, 10 256 (1993).
[14] See EPAPS Document No. E-PRLTAO-97-065652 for the EPAPS supplementary materials showing the details of the derivation of Eq. (6). For more information on EPAPS, see http://www.aip.org/pubservs/epaps.html.
[15] I. Gerhardt *et al.* (to be published).
[16] M. A. Lieb, J. M. Zavislan, and L. Novotny, J. Opt. Soc. Am. B **21**, 1210 (2004).
[17] D. R. Lytle II, P. S. Carney, J. C. Schotland, and E. Wolf, Phys. Rev. E **71**, 056610 (2005).
[18] S. Kühn, U. Håkanson, L. Rogobete, and V. Sandoghdar, Phys. Rev. Lett. **97**, 017402 (2006).
[19] S. J. van Enk and H. J. Kimble, Phys. Rev. A **63**, 023809 (2001).
[20] P. Horak *et al.*, Phys. Rev. A **67**, 043806 (2003).
[21] Q. A. Turchette, C. J. Hood, W. Lange, H. Mabuchi, and H. J. Kimble, Phys. Rev. Lett. **75**, 4710 (1995).